Combining SAR tomography and a PSI approach for high-resolution 3-D imaging of an urban area

Othmar Frey
Earth Observation & Remote Sensing, ETH Zurich, Switzerland / Gamma Remote Sensing, Gümligen, Switzerland
Email: otfrey@ethz.ch

Muhammad Adnan Siddique
Earth Observation & Remote Sensing, ETH Zurich, Switzerland

Irena Hajnsek
Earth Observation & Remote Sensing, ETH Zurich, Switzerland / German Aerospace Center - DLR, Germany

Urs Wegmüller, Charles L. Werner
Gamma Remote Sensing, Gümligen, Switzerland

Abstract

Combining persistent scatterer interferometry (PSI) and SAR tomography approaches has the potential to overcome layover scenarios in urban areas and may thus increase the level of detail of differential interferometric measurements of displacements in such environments. In this paper, we report the current status and results of our efforts to integrate SAR tomography into an operational interferometric point target analysis (IPTA) processing tool as an extension to the conventional persistent scatterer interferometry approach. In particular, the PSI and the SAR tomography processing approaches applied are highlighted. In addition, details in the form of tomographic slices of two high-rise buildings are presented as well as a 3-D point cloud reconstruction of parts of the city of Barcelona are shown, as extracted from an interferometric stack of high-resolution stripmap-mode SAR data at X-band acquired by the TerraSAR-X spaceborne SAR sensor.

1 Introduction

Interferometric stacks of high resolution synthetic aperture radar (SAR) data over urban areas yield a high number of scatterers that are stable over a long time span. The high resolution also leads to a higher probability of multiple temporally coherent scatterers occurring in the same range-azimuth resolution cell. Conventional persistent scatterer interferometry is based on the assumption that only one scatterer is present in a particular resolution cell. SAR tomography has the potential to overcome this restriction. In this contribution, we explore a TerraSAR-X stack over the city of Barcelona in terms of computationally efficient approaches such as Tikhonov-regularized inversion for tomographic focusing and a local peak detection for detection of scatterer localization.

Exploitation of the elevation dimension through SAR tomography approaches adds valuable information about the structure of complex target scenarios. Potential example applications include forest parameter retrieval, retrieval of structure information in urban areas, and retrieval of additional coherent targets in such scenarios. 3-D tomographic processing of such scenarios from multibaseline SAR data has been addressed and discussed by a number of authors [1–4] and [5–12]. In the spaceborne case, ideally 25–50 or up to 100 repeat-pass interferometric data sets of the same area with spatial baselines perpendicular to the line of sight are required to resolve targets also in the elevation direction, or potentially even in space and time. In this paper we show the status and results of our efforts to integrate SAR tomography into an operational interferometric point target analysis (IPTA) software as an extension to the conventional persistent scatterer interferometry approach.

2 Methods

The repeat-pass nature of the spaceborne interferometric stack requires that, prior to be able to perform SAR tomography in the elevation direction, a PSI processing sequence is performed to extract and remove the atmospheric phase contributions [13]. This preprocessing sequence comprises of the selection of a reference scene from stack of single-look complex (SLC) images, geocoding the data using the multilook intensity image of the reference scene, and co-registration including a refinement step using offset estimates between the data sets of the stack. After a preselection of point target candidates, based on spectral diversity and the temporal variability of the backscattering, point differential interferograms are calculated, iteratively. The topographic and orbital phases are then simulated and subtracted from the point-wise complex-valued interferogram followed by unwrapping and filtering to isolate the spatially correlated phase contributions from high-frequency phase contributions such as the residual topographic phase. If an acceptable PSI solution has been reached, the low-

ISBN 978-3-8007-3607-2 / ISSN 2197-4403

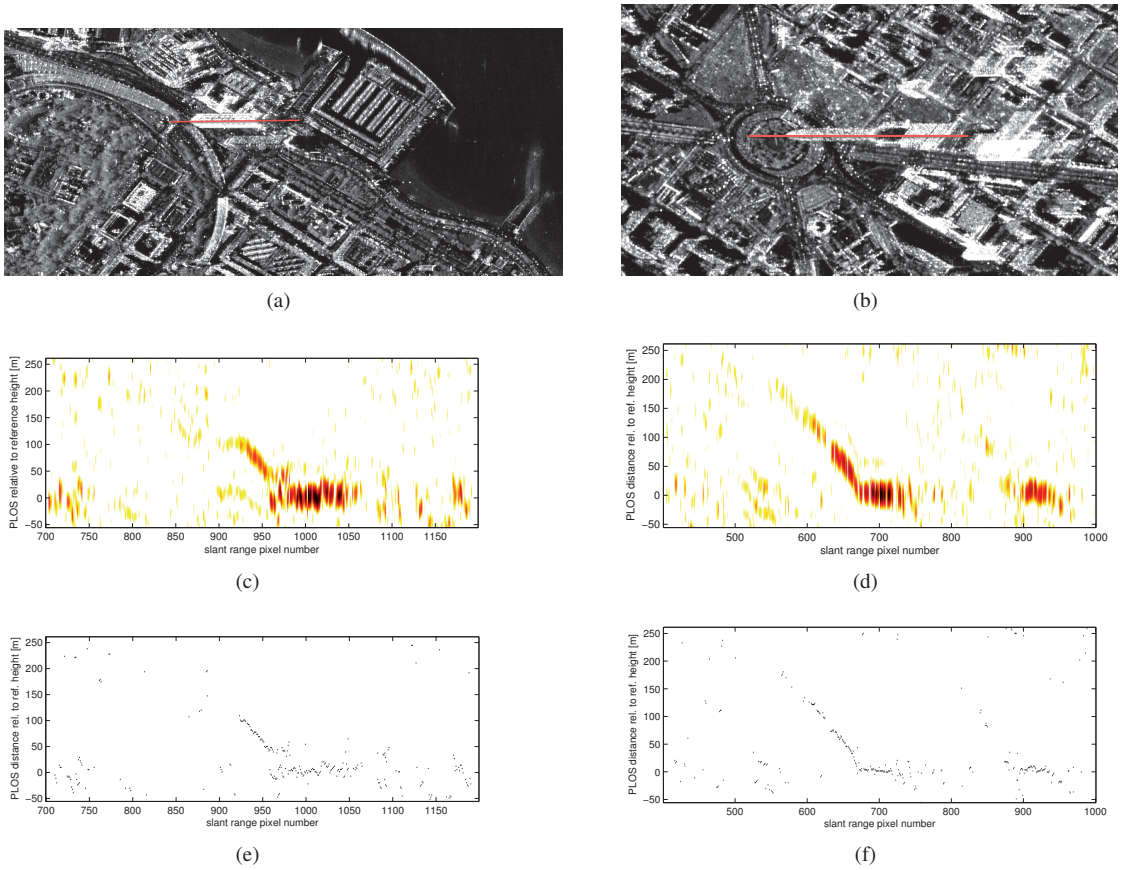

Figure 1: Top row: Subsets of the temporally averaged intensity image of the TerraSAR-X interferometric stack showing the layover situation for a tower close to the Olympic Village in Barcelona (a) and for the Torre Agbar and surrounding buildings (b). Middle row: Tomographic slices showing the resolved extended layover situation in the slant range / elevation plane for the tower near the Olympic Village (c) and the Agbar Tower (d). Tomographic focusing algorithm: single-look Tikhonov-regularized inversion. Bottom row (e) and (f): The associated extracted locations of stable scatterer candidates using a 2-peak detector.

frequency phase contributions are expanded to the full SLCs again, such that tomographic focusing can potentially be performed at each pixel location in the SLC to find multiple scatterers in one range-azimuth resolution cell.

In the following, the system model and the tomographic inversion approaches are sketched.

The complex reflectivity s of a point target source can be described as

$$s = \alpha e^{i\phi}, \tag{1}$$

where α is the amplitude and ϕ is the phase of s. So the complex demodulated signal vector $\mathbf{y}$ for that particular source s yields

$$\mathbf{y} = \mathbf{a}s \tag{2}$$

where $\mathbf{a} = [1\, e^{i\varphi_2} \dots e^{i\varphi_K}]^T$ is the steering vector with $\varphi_m = -2k_c(r_m - r_1)$, $m = 1 \dots K$; k_c is the central wavenumber and r_m is the range distance from the point scatterer to the m-th sensor position.

Then, for p point target sources the signal vector $\mathbf{y}$, which represents the signal impinging on the antenna array synthesized by the different locations of the various SLC acquisition in elevation direction is

$$\mathbf{y} = \begin{bmatrix} \mathbf{a}_1 & \dots & \mathbf{a}_p \end{bmatrix} \begin{bmatrix} s_1 \\ \vdots \\ s_p \end{bmatrix} = \mathbf{B}\mathbf{s}. \tag{3}$$

The matrix $[\mathbf{a}_1 \dots \mathbf{a}_p]$ is translated to matrix $\mathbf{B}$ called the steering matrix.

A straight-forward reconstruction—the beamforming case—of the complex reflectivity $\hat{\mathbf{s}}$ along the elevation direction is obtained by

$$\hat{\mathbf{s}} = \mathbf{B}^H \mathbf{y} \tag{4}$$

The sampling of the tomography data is non-uniform in the elevation direction. Therefore the reconstructed tomographic profile is typically affected by spurious side lobes. A method that provides a regularized tomographic inversion is the truncated singular value decomposition (TSVD) approach as it has been suggested and applied in the context of SAR tomography in [14]. It starts with a singular

ISBN 978-3-8007-3607-2 / ISSN 2197-4403

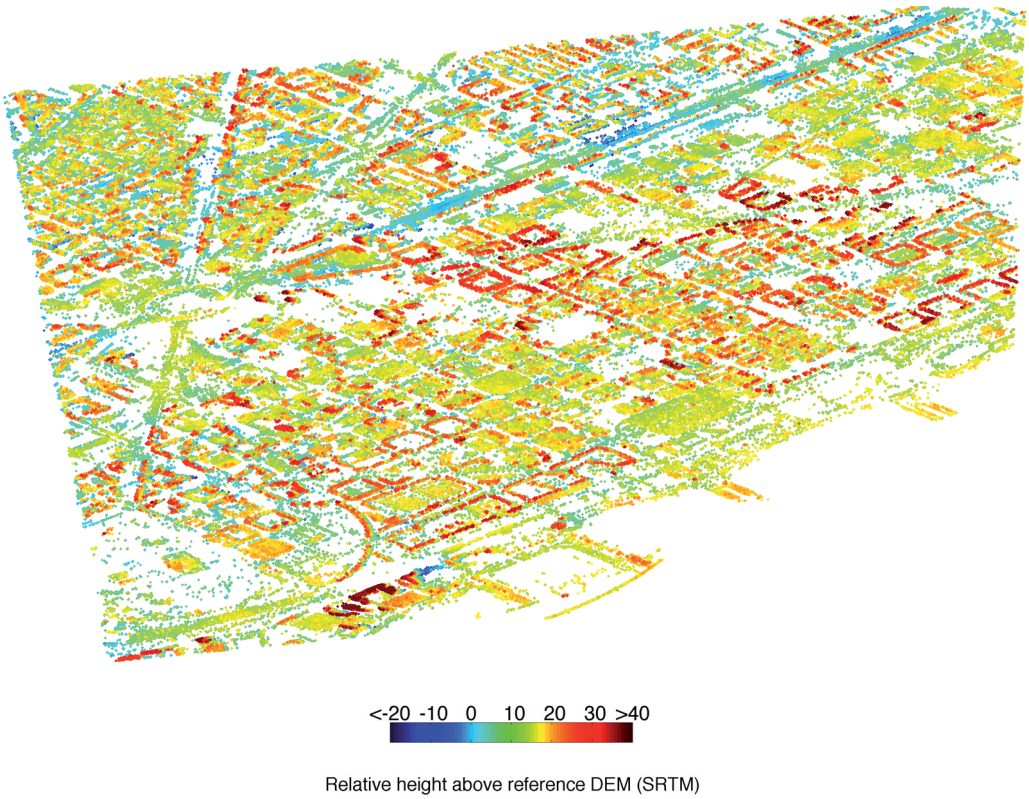

Figure 2: Extracted 3-D point cloud based on Tikhonov-regularized tomographic inversion of a stack of 45 stripmap-mode TerraSAR-X single look complex images acquired over the city of Barcelona. The colour coding indicates the height of the scatterer relative to the SRTM height model, which is used as a reference.

value decomposition of the steering matrix $\mathbf{B} = \mathbf{U}\mathbf{\Sigma}\mathbf{V}^H$. A noise threshold is set at the Q-th singular value as a function of the decay pattern of the singular values σ_n in the diagonal matrix Σ. All singular values $\sigma_n, n = Q+1, ..., K$ that lie below this threshold, as well as their corresponding orthogonal vectors $\mathbf{u}_n$, $\mathbf{v}_n$, are discarded. The tomographic profile is then calculated by means of the truncated pseudo-inverse $\mathbf{V}_{1,Q}(\mathbf{\Sigma}^{-1})_{1,Q}\mathbf{U}_{1,Q}^H$ of the steering matrix $\mathbf{B}$:

$$\hat{\mathbf{s}} = \mathbf{V}_{1,Q}(\mathbf{\Sigma}^{-1})_{1,Q}\mathbf{U}_{1,Q}^H\mathbf{y} \tag{5}$$

$\mathbf{B}$ is the steering matrix of size $K \times N_r$, where K is the number of acquisitions and N_r is the number of the regularly sampled positions of the tomographic profile in elevation direction.

Another approach to regularize the inversion is the Tikhonov-regularization. Instead of cutting the noise space the inverse singular values $\sigma_{n_{rt}}^{-1}$ are weighted according to the following scheme

$$\sigma_{n_{rt}}^{-1} = \frac{\sigma_n}{\sigma_n^2 + \epsilon^2}, \quad \epsilon = \sqrt{\frac{K}{K-Q}\sum_{n=Q+1}^{K}|\mathbf{U}_{Q+1,K}^H\mathbf{y}|^2} \tag{6}$$

where ϵ^2 is the noise power level estimated from the projection of the measured data to the noise space [4].

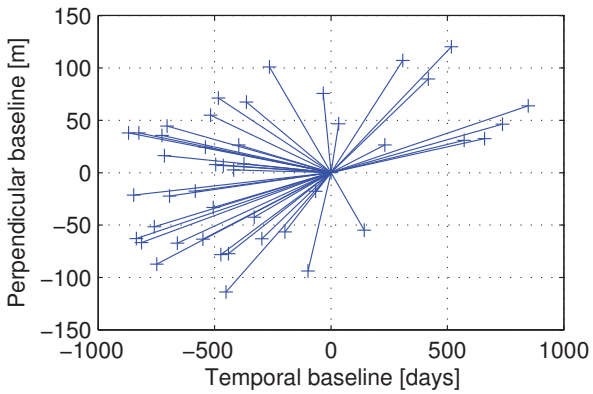

Figure 3: Temporal vs. perpendicular spatial baseline with respect to the reference track.

3 Data

An interferometric stack of TerraSAR-X stripmap-mode data over the city of Barcelona is used for the combined PSI and tomographic processing. The single-reference stack consists of 45 SLCs that were acquired between 2008 and 2012. In Fig. 3, the temporal and spatial perpendicular baseline distribution of the data tomographic data set is visualized.

ISBN 978-3-8007-3607-2 / ISSN 2197-4403

4 Results

Figs. 1 (a) and (b) show two excerpts of the TerraSAR-X data set over the city of Barcelona as a temporally averaged multi-look intensity image. In Figs. 1 (c) and (d) the corresponding tomographic transects in range/elevation depicting the tomographically resolved layover situation given by the two high-rise buildings are shown. Figs. 1 (e) and (f) show the extracted point target locations as obtained from the tomographic profiles in elevation direction. In Fig. 2 a 3-D point cloud of a larger district of Barcelona is shown as extracted using threshold-aided peak-finding within the tomographic profiles.

5 Discussion and Outlook

The tomographic slices in the elevation direction, obtained based on Tikhonov-regularized tomographic inversion, show that the layover situation induced by the high-rise buildings is resolved with a good side-lobe suppression. The Tikhonov-regularized inversion is computationally efficient; a drawback is the limited resolution compared to, e.g., compressive sensing approaches, which in contrast are computationally expensive. The 3-D point cloud extracted from the tomographic inversion of the stack of TerraSAR-X data shows a tomographic reconstruction of a district of Barcelona revealing a high level of detail of building structures and infrastructure features. The processing scheme presented is currently undergoing a consolidation phase, in which the benefit of the combined PSI/tomography approach in terms of an improved deformation monitoring in the context of the IPTA processing scheme [13] is further investigated.

Acknowledgment

This research project is funded by the Swiss Space Office, State Secretariat for Education and Research of the Swiss Confederation (SER/SSO), through the MdP2012 initiative. TerraSAR-X SAR data over Barcelona was obtained courtesy of the German Aerospace Center DLR through proposal MTH1717. SRTM ©USGS.

References

[1] G. Fornaro and A. Pauciullo, "LMMSE 3-D SAR focusing," *IEEE Trans. Geosci. Remote Sens.*, vol. 47, no. 1, pp. 214–223, Jan. 2009.

[2] G. Fornaro and F. Serafino, "Imaging of single and double scatterers in urban areas via SAR tomography," *IEEE Trans. Geosci. Remote Sens.*, vol. 44, no. 12, pp. 3497–3505, 2006.

[3] S. Sauer, L. Ferro-Famil, A. Reigber, and E. Pottier, "Three-dimensional imaging and scattering mechanism estimation over urban scenes using dual-baseline polarimetric InSAR observations at L-band," *IEEE Trans. Geosci. Remote Sens.*, vol. 49, no. 11, pp. 4616–4629, Nov. 2011.

[4] X. X. Zhu and R. Bamler, "Very high resolution spaceborne SAR tomography in urban environment," *IEEE Trans. Geosci. Remote Sens.*, vol. 48, no. 12, pp. 4296–4308, Dec. 2010.

[5] A. Reigber and A. Moreira, "First demonstration of airborne SAR tomography using multibaseline L-band data," *IEEE Trans. Geosci. Remote Sens.*, vol. 38, no. 5, pp. 2142–2152, 2000.

[6] O. Frey and E. Meier, "Analyzing tomographic SAR data of a forest with respect to frequency, polarization, and focusing technique," *IEEE Trans. Geosci. Remote Sens.*, vol. 49, no. 10, pp. 3648–3659, Oct. 2011.

[7] O. Frey and E. Meier, "3-D time-domain SAR imaging of a forest using airborne multibaseline data at L- and P-bands," *IEEE Trans. Geosci. Remote Sens.*, vol. 49, no. 10, pp. 3660–3664, Oct. 2011.

[8] O. Frey, F. Morsdorf, and E. Meier, "Tomographic Imaging of a Forested Area By Airborne Multi-Baseline P-Band SAR," *Sensors, Special Issue on Synthetic Aperture Radar*, vol. 8, no. 9, pp. 5884–5896, sep 2008.

[9] O. Frey, I. Hajnsek, and U. Wegmuller, "Spaceborne SAR tomography in urban areas," in *Proc. IEEE Int. Geosci. Remote Sens. Symp.*, 2013, pp. 69–72.

[10] E. Aguilera, M. Nannini, and A. Reigber, "Multisignal compressed sensing for polarimetric SAR tomography," *IEEE Geosci. Remote Sens. Lett.*, vol. 5, no. 9, pp. 871–875, Sept. 2012.

[11] S. Tebaldini, "Single and multipolarimetric SAR tomography of forested areas: A parametric approach," *IEEE Trans. Geosci. Remote Sens.*, vol. 48, no. 5, pp. 2375–2387, May 2010.

[12] M. Nannini, R. Scheiber, R. Horn, and A. Moreira, "First 3-D reconstructions of targets hidden beneath foliage by means of polarimetric SAR tomography," *IEEE Geosci. Remote Sens. Lett.*, vol. 9, no. 1, pp. 60 –64, Jan. 2012.

[13] U. Wegmuller, D. Walter, V. Spreckels, and C. Werner, "Nonuniform ground motion monitoring with TerraSAR-X persistent scatterer interferometry," *IEEE Trans. Geosci. Remote Sens.*, vol. 48, no. 2, pp. 895 –904, Feb. 2010.

[14] G. Fornaro, F. Serafino, and F. Soldovieri, "Three-dimensional focusing with multipass SAR data," *IEEE Trans. Geosci. Remote Sens.*, vol. 41, no. 3, pp. 507–517, 2003.

ISBN 978-3-8007-3607-2 / ISSN 2197-4403